Hindawi
Journal of Sensors
Volume 2020, Article ID 5932539, 12 pages
https://doi.org/10.1155/2020/5932539

Research Article

Netted Radar Tracking with Multiple Simultaneous Transmissions against Combined PDS Interception

Zijian Wu, Fei Wang, and Jianjiang Zhou

College of Electronic and Information Engineering, Nanjing University of Aeronautics and Astronautics, Nanjing 211106, China

Correspondence should be addressed to Fei Wang; wangxiaoxian@nuaa.edu.cn

Received 20 August 2019; Revised 7 December 2019; Accepted 18 December 2019; Published 4 January 2020

Academic Editor: Stelios M. Potirakis

One of the advantages of a netted airborne radar system (NARS) is escaping interception of the passive detection system (PDS) while tracking a target. A significant tactic to realize tracking without PDS interception is to study the low probability of interception (LPI) time of NARS. Firstly, this paper analyses the power, frequency, and platform interception probabilities of a combined PDS consisting of a radar-warning receiver (RWR) and an electronic support measurement (ESM). Secondly, this paper takes interactive multiple models (IMM) to describe the target tracking process and introduces a binary hypothesis test for chi square as well as noncentralized chi square distributions as a detection criterion of NARS during target tracking after the design of adaptive dwell time and the maximum illumination interval algorithm. Finally, based on experiential moving platform interception probabilities of a RWR and an ESM, a simplified math model is presented to estimate LPI time of NARS when the parameters are partially known. Simulations illustrate that the simultaneous management of radiation power and time is crucial for NARS against combined PDS interception.

1. Introduction

Low probability of interception (LPI) technologies are necessary for an advanced aircraft to protect itself from a passive detection system (PDS) [1–3]. In order to improve the surviving ability of aircrafts, the airborne radar has to take advantage of LPI tactics to conceal its positions and action purposes.

As for the radiation power control of a phased-only array radar, Zhang and Zhu proposed a multilevel power control strategy which showed better tracking performance and radiation power saving [4]. Kamble et al. analysed the relationship between emission power and target identification rate with a phase-coded radar waveform based on high resolution range profile (HRRP) [5]. Shi et al. designed a scheme to allocate power based on LPI radar in a complex electromagnetic background [6]. Wang et al. studied the joint allocation of beam pointing and dwell time of phased array radar in multitarget tracking [7]. Shi et al. proposed an optimized method of parameters including radar's illumination interval, dwell time, and radiated power in target tracking, which showed the achievement of minimum interception probability [8]. And the illumination interval represents the time gap between two consecutive illuminations of the radar system transmitters.

The ESM with a frequency search mode has a relatively longer intercept range than the detection range of radar so that the probability of interception in the power domain can be considered independent of range. We then assume that the ESM's power interception probability equals to one when the radar is transmitting signals. However, the bandwidth of the ESM is narrow compared with the search range; thus, the frequency interception probability is very low. On the other hand, the RWR has a wider bandwidth compared with the ESM, and the frequency interception probability can be considered 100% when the radar is transmitting signals. However, its power intercept ability grew in inverse proportion to the distance between radar and target. Then, the netted airborne radar system (NARS) is attracting more and more researchers' attention; each radar NARS can not only detect targets independently but also be managed by some fusion rules cooperatively. NARS always include different types of radar nodes, which can work under different mechanisms, frequency bands, working modes,

and polarization modes. After fusing data from all radar nodes, NARS can improve the detection and LPI performances at the same time. The general rules to improve LPI performance of NARS are to allocate its power, time, and antenna resources reasonably. Godrich et al. proposed a power resource allocation scheme to meet the localization accuracy by minimizing the total transmitted energy of NARS [9]. Chavali and Nehorai studied a competitive resource allocation tactic of NARS using game theory [10]. Gao et al. proposed three allocation schemes about resources of NARS to improve its target detection performance by combining antenna and dwell time resources [11]. Barbary and Zong deduced a maximum nonparametric detection performance of NARS, which can be used to control radiation power when targets' distances are known [12]. Shi et al. and Liu et al. proposed an effective way to minimize the intercept factor while maintaining tracking performance, and results proved it worked well [13, 14]. And the intercept factor can evaluate the LPI performance of the radar network system. Wang et al. proposed a track mission shifting tactic of a distributed airborne radar system or distributed airborne formation radar system based on LPI time [15]. And the LPI time refers to the time during which a certain airborne radar system is tracking the target without being intercepted by a passive detection system.

The resource management models and algorithms of NARS are similar to the MIMO radar system. As for the MIMO radar system, Song et al. integrated the propagation losses into the MIMO radar signal model and investigate the power allocation problems [16]. Liao et al. proposed an interception probability model of the MIMO radar system by analysing radar signals in time, frequency, space, and power domains [17]. Yang et al. optimized LPI performance of the MIMO radar system by allocating its antenna, power, and dwell time resources in models of searching and detecting MIMO radar system [18]. Yu et al. improved the performance gain of CS-MIMO radars by allocating optimal power among the transmit antennas [19]. Garcia et al. proposed an algorithm to allocate power and bandwidth of the MIMO radar system reasonable with CRLB, which can get the best localization performance of multiple targets [20]. Ma et al. considered a joint scheme of antenna subset selection and optimal power allocation, and results showed better localization performance compared with other strategies and were close to the optimal solution [21]. Considering prior knowledge, Yan et al. studied the allocation of radar resources for different purposes when the MIMO radar system tracks multiple targets [22, 23]. A maximum signal-to-interference-plus-noise ratio (SINR) based on frequency diverse property of the MIMO radar system was deduced by Xiang and Chen, which was designed to control the power of the MIMO radar system under a determined SINR [24]. Tang et al. designed a new MIMO radar waveform which was used to improve the Rician targets' detection performance under a limited power [25].

However, most papers are in lack of radiation time analysis of NARS because of the common assumption that the passive detection system is unknown, which leads to the absence of LPI time analysis. Since modern intelligence system and early warning system have made it possible for NARS to obtain some properties of a PDS, this paper attempts to study LPI time of NARS when those properties are partially known. Some work has been done in [15], which only took the ESM into account. For the reason that modern aircraft are always equipped with both a RWR system and an ESM system, this paper takes a combined PDS made of the two systems into account. Since the probability of intercept of the ESM is independent of range and the RWR has an intercept ability that grew in inverse proportion to the distance between radar and target, the paper took different characteristics of the RWR and the ESM into account and changed the optimum LPI detection strategy of the network against interception. The simulations assume that NARS composed of four radars formed a square formation moving towards the target. Firstly, through deducing the short-time interception probability of the ESM based on the adaptive time resource constraint by NARS, this paper defines a platform interception probability of a combined PDS as the function of the radiation time by NARS, the power interception probability of a RWR, and the frequency interception probability of an ESM. Secondly, considering the definition of platform interception probability, this paper establishes a simplified math model to study the LPI time of NARS under some assumptions of experiential moving platform interception probabilities of a combined PDS.

The main contributions of this paper are as follows: (1) This paper establishes a math model to analyse the LPI time of NARS confronting a combined PDS made of a RWR and an ESM. (2) Corresponding to the maximum illumination interval tactic adopted by NARS, this paper proposes a short-time average interception probability to replace the common interception probability of an ESM.

2. Platform Interception Probability Model of a Combined PDS

Based on previous work of other researchers, this paper assumed that the tracking ability of the network can well meet the task requirements. Relating works [26, 27] are as follows: Goodman used the likelihood ratio test (LRT) for multistatic airborne radar detection; the simulation results showed that diversity and geometry gain could be achieved through multistatic space-time adaptive processing (STAP). Rong et al. proposed a multiple access protocol for intraflight data link which meets the high-speed, secure, and reliable information sharing between the planes. This paper assumes that NARS is composed of N_t transmitters and N_r receivers, and each of which can independently transmit and process orthogonal waveforms at the same time. The main lobe of each radar antenna of NARS is tracking the target equipped with a combined PDS. Only a radiation signal of NARS satisfies the detected conditions of power, spatial, frequency, and time domains. The general detection probability P_i of a signal emitted by NARS could be expressed as

$$P_i = P_s \cdot P_f \cdot P_d \cdot P_t, \tag{1}$$

where P_s, P_f, P_d, and P_t denote detection probabilities of spatial, frequency, power, and time domains.

As for the RWR designed to detect radar signals instantly as soon as possible in a confrontation scene, both P_s and P_t in equation (1) should approximately equal to 1 because the platform of radar would not move quickly in the space domain and the radar signal would hold on for a while in the time domain. However, there have to be a trade-off between P_f and P_d because of the physical contradictory relationship between the bandwidth and sensitivity of a RWR or an ESM. To reduce that contradiction and improve the performance of the passive detection system, an effective method is to combine the high-sensitivity narrow-band ESM and the low-sensitivity wide-band RWR.

2.1. Power Interception Probability of a RWR. According to equation (1), both P_f and P_d are significant for the combined PDS; a low-sensitivity wide-band RWR is suitable to model the property of P_d of the combined PDS. Considering a classical detection equation of a linear detector, the interception probability of the RWR could be expressed as [28]

$$P_d = 2\int_{\sqrt{-\ln(P_{fa})}}^{\infty} y \cdot \exp\left(-\left(y^2 + \mathrm{SNR}_i\right)\right) I_0\left(2y\sqrt{\mathrm{SNR}_i}\right) dy, \tag{2}$$

where P_{fa} is the false alarm possibility, I_0 denotes the modified first-order Bessel function, and SNR_i represents the signal to noise (SNR) ratio. When SNR_i is larger than 6 dB, a classical approximate expression [29] of equation (2), that is,

$$P_d = 0.5 \cdot \mathrm{erfc}\left(\sqrt{-\ln p_{fa}} - \sqrt{\mathrm{SNR}_i + 0.5}\right),$$
$$\mathrm{erfc}(z) = 1 - \frac{2}{\sqrt{\pi}}\int_0^z e^{-v^2} dv. \tag{3}$$

This paper proposes to use P_d, P_{fa}, and SNR_i of equation (3) to model the interception performance in the power domain of the combined PDS.

2.2. Frequency Interception Probability of an ESM. Equation (3) shows interception performance in the power domain by a RWR of the combined PDS. Then, this paper proposes to describe the frequency interception property P_f by an ESM. Frequency search is the most popular search mode of the ESM, and the average interception time on the frequency domain is widely used to describe an ESM performance. The relationship between it and interception is that the shorter the average interception time is, the higher the interception probability of an ESM will be.

Due to the high sensitivity of ESM in the frequency search mode, this paper suggests that $P_s = 1$, $P_d = 1$, and $P_t = 1$. Therefore, the interception probability of a high-sensitivity ESM is defined as

$$p_{f_i} = \frac{\Delta f_s}{B_s}, \tag{4}$$

where Δf_s is ESM's stepping frequency and B_s is an ESM's frequency search range and is greater than the radar's frequency hopping range. Supposing that there are N_t radars in NARS transmitting orthogonal waveforms with N_t' ($N_t' \le N_t$) carrier frequencies at the same time, then the intercepted probability of NARS by an ESM could be

$$p_f = 1 - \left(1 - p_{f_i}\right)^{N_t'}. \tag{5}$$

If $N_t' p_{f_i} < 0.3$, equation (5) could be approximated as

$$p_f \approx N_t' p_{f_i}. \tag{6}$$

Then, the ESM search period is

$$T_f = \frac{\tau_{rem}}{p_f} = \frac{\tau_{rem}}{N_t' p_{f_i}}, \tag{7}$$

where T_f is the frequency search period and τ_{rem} is dwell time of an ESM. When the illumination period is a constant, the interception definition of the ESM can be given by De Martino [30]. However, NARS often need to track the target with an adaptive illumination interval; thus, the short-time average interception time of the ESM is

$$\bar{T}_c = \frac{T_f \bar{T}_{rs}}{\tau_e' - \tau_{rem}}, \tag{8}$$

where $\bar{T}_{rs}$ and $\tau_e' = \tau_e/(N_t)^\eta$ are the short-time average illumination interval and dwell time of NRAS on the target, respectively. Let $0.5 \le \eta < 1$ represent noncoherent integration efficiency, τ_e denotes the sum of dwell time of NARS; thus, the NARS's short-time average intercepted probability by an ESM is

$$P_f(x) = \begin{cases} 1 - \exp\left(-\dfrac{x}{\bar{T}_c}\right), & x > 0, \\ 0, & x < 0, \end{cases} \tag{9}$$

where x denotes the total scan time of ESM.

If $\bar{T}_{rs}$ is a constant, equation (8) can be rewritten as

$$\bar{T}_c \propto \frac{\tau_{rem}}{N_t' p_{f_i}}\left(\frac{\tau_e}{(N_t)^\eta - \tau_{rem}}\right). \tag{10}$$

If $N_t = N_t' = 1$, then

$$\bar{T}_c \propto \frac{\tau_{rem}}{p_{f_i}(\tau_e - \tau_{rem})}. \tag{11}$$

Since τ_{rem} are smaller than τ_e and $\tau_e/(N_t)^\eta$, if $(N_t)^\eta \geq N_t'$, then

$$N_t' p_{f_i}\left(\frac{\tau_e}{(N_t)^\eta} - \tau_{\text{rem}}\right) \leq p_{f_i}(\tau_e - \tau_{\text{rem}}), \tag{12}$$

which means that the LPI performance of NARS is proportional to the number of aircrafts in NARS. Equations (10) and (11) show that minimizing the number of carrier frequencies and minimizing radiation time of NARS are good ways to escape from a high-sensitivity ESM with a frequency search mode.

2.3. Platform Interception Probability of a Combined PDS. Although LPI performance is important to protect NARS from combined PDS, NARS must use a reasonable SNR to detect targets. Thus, SNR_{net} of NARS is defined as the ideal coherent integration for all radar nodes, that is,

$$\text{SNR}_{\text{net}} = \sum_{i=1}^{N_t}\sum_{j=1}^{N_r} \text{SNR}_{ij}, \tag{13}$$

where $\text{SNR}_{ij} = P_{ti}G_{ti}G_{rj}G_{rpj}\sigma_{ij}\lambda_i^2\tau_{\text{ei}}/(4\pi)^3 kT_oB_{ri}F_{ri}R_{ti}^2R_{rj}^2L_{ij}$ T_{ri}, P_{ti}, G_{ti}, τ_{ei}, T_{ri}, λ_i, B_{ri}, and F_{ri} are emission power, antenna gain, dwell time, pulse repetition time, wavelength, bandwidth of match filter, and noise coefficient of the ith radar; G_{rj} and G_{rpj} represent antenna gain and processor gain of the jth radar receiver; σ_{ij} is radar cross-section (RCS) of a target between the ith radar and the jth radar receiver; k is Boltzmann constant; T_o is system noise temperature; L_{ij} is system loss between the ith radar and the jth radar; R_{ti} is distance from the ith radar to the target; and R_{rj} is distance between the target and the jth radar. If the coherent integration process of NARS is not perfect, that loss could be reflected in L_{ij}.

3. The Analysis of LPI Time for NARS

3.1. The Design of Adaptive Dwell Time and Illumination Interval. In NARS, we use the binary hypothesis test to analyse H_0 and H_1, which are centralized chi square distribution and noncentralized chi square distribution, respectively,

$$\begin{cases} H_0 : r \sim \chi^2\left(N_t^2\right), \\ H_1 : r \sim \chi'^2\left(N_t^2\right). \end{cases} \tag{14}$$

After match filtering, the time when jth radar gets the max output is t_0. In equation (14), for H_0, $E(r) = N_t^2$ and var $(r) = 2N_t^2$ are the mean and variance of r. For H_1, the mean and variance are $E(r) = N_t^2 + \lambda$ and var $(r) = 2N_t^2 + 4\lambda$, $\lambda = \sum_{j=1}^{N_t}\sum_{k=1}^{N_t}\mu_{jk}^2(t_0)$. When $t = t_0$, the mean is $\mu_{jk}(t_0)$. For H_0, $\mu_{jk}(t_0) = 0$. And λ is determined by the minimum acceptable SNR_{net}.

In this paper, adaptive dwell time and illumination interval design are mutually independent, so the NARS system can control the dwell time to meet the requirement of the tracking task. After estimating the information of RCS and the target distance, NARS first adjust the dwell time to satisfy required SNR_{net} for H_1 in equation (14). Since the estimation values are not exactly accurate, the NARS will continue to illuminate the target for $\Delta\tau_e$ until the hypothesis test H_1 is available if the current dwell time cannot meet the requirement.

The following is a classic adaptive illumination interval design process [31]. The state and measure equations of the jth move model of the target are defined as

$$\hat{X}_j(t) = F_j^{\Delta T}X_j(t - \Delta T) + V_j^{\Delta T}(t), \tag{15}$$

$$Z(t) = H_j^{\Delta T}X_j(t) + W_j^{\Delta T}(t), \tag{16}$$

where $\hat{X}_j(t)$ and $X_j(t)$ are predicted state vector and state vector of the jth model; $Z(t)$ is measure vector at time t; and $F_j^{\Delta T}$, $H_j^{\Delta T}$, $V_j^{\Delta T}(t)$, and $W_j^{\Delta T}(t)$ are the transfer matrix, measure matrix, system noise, and measure noise of the jth model, respectively, when the illumination interval of the radar transmitter is ΔT, which is the time gap between two consecutive illuminations of the NARS transmitters. $\Delta T = m\Delta T_{\min}$, $m \in [1, 2, \cdots, M]$, where $\Delta T_{\min}$ and $M\Delta T_{\min}$ are the minimum and the maximum intervals available. Covariance matrices of $V_j^{\Delta T}(t)$ and $W_j^{\Delta T}(t)$ are $Q_j^{\Delta T}(t)$ and $R_j^{\Delta T}(t)$, respectively.

Adaptive illumination interval design based on the interactive multimodel Kalman filter (IMMKF) process is as follows after combining with equations (15) and (16).

Step 1. Supposing ΔT is the illumination interval from the previous time to current time and the posterior state vector $\hat{X}_j(t - \Delta T)$ of the jth model of last time is

$$\hat{X}_j(t - \Delta T) = \sum_{i=1}^{r}\hat{X}_i(t - \Delta T)\cdot\mu_{i|j}(t - \Delta T), \tag{17}$$

where $\mu_{i|j}(t)$ is the model converting probability of the jth model transferred from the ith model.

Step 2. According to the following formula to compute predicted covariance error matrix $P_j^{\Delta T}(t^-)$, residual matrix $S_j^{\Delta T}(t)$, and Kalman gain $K_j^{\Delta T}(t)$ of the jth model,

$$\begin{aligned} P_j^{\Delta T}(t^-) &= F_j^{\Delta T}P_j(t - \Delta T)\left(F_j^{\Delta T}\right)^T + G_j^{\Delta T}Q_j^{\Delta T}(t)\left(G_j^{\Delta T}\right)^T, \\ S_j^{\Delta T}(t) &= H_j^{\Delta T}P_j^{\Delta T}(t)\left(H_j^{\Delta T}\right)^T + R_j^{\Delta T}(t), \\ K_j^{\Delta T}(t) &= P_j^{\Delta T}(t^-)\left(H_j^{\Delta T}\right)^T\left[S_j^{\Delta T}(t)\right]^{-1}, \end{aligned} \tag{18}$$

where $P_j(t-\Delta T)$ denotes the covariance error matrix of last time and $G_j^{\Delta T}$ denotes the weighing matrix of system noise of the jth model.

Step 3. Estimating state vector $\hat{X}_j(t)$ and covariance error matrix $P_j(t)$ of the jth model by using Step 2's result:

$$\begin{aligned}\hat{X}_j(t) &= F_j^{\Delta T}\hat{X}_j(t-\Delta T) + K_j^{\Delta T}(t) \\ &\quad \cdot \left[Z(t) - H_j^{\Delta T}F_j^{\Delta T}\hat{X}_j(t-\Delta T)\right], \\ P_j(t) &= I - K_j^{\Delta T}(t)H_j^{\Delta T}P_j^{\Delta T}(t^-),\end{aligned} \tag{19}$$

where I denotes the unit matrix.

Step 4. Updating each moving model's probability:

$$\mu_j(t) = \frac{\Lambda_j(t)\sum_{i=1}^{r}\pi_{ij}\mu_i(t-1)}{\sum_{j=1}^{r}\sum_{i=1}^{r}\Lambda_{j(t)\pi_{ij}\mu_i(t-1)}}, \tag{20}$$

where $\Lambda_j(t)$ is likelihood function of the jth model at time t; π_{ij} is transform probability from the ith model to the jth model, $\sum_{i=1}^{I}\pi_{ij} = 1, i = 1, 2, \cdots, I$; and $\mu_i(t)$ is probability of the jth model at time t.

Step 5. Combining state vectors and covariance error matrices of all models to $\hat{X}(t)$ and $P(t)$:

$$\begin{aligned}\hat{X}(t) &= \sum_{j=1}^{r}\hat{X}_j(t)\mu_j(t), \\ P(t) &= \sum_{j=1}^{r}\mu_j(t)\left(P_j(t) + b_j b_j^{\,T}\right),\end{aligned} \tag{21}$$

where $b_j = [\hat{X}_j(t) - \hat{X}(t)]$.

In Steps 1–5, a process cycle of IMMKF is finished, and predicted upper limitation $P^{\text{pred}}(t)$ determines illumination interval ΔT. Then, repeat Steps 1–5 to continue the next adaptive illumination interval.

3.2. LPI Time for NARS. According to the property of a RWR, the location error of the signal source is relatively large using the amplitude location algorithm so that a relatively long time about 20 to 100 seconds is needed to initialize tracking of the platform of the signal source. On the contrary, with the phase location algorithm, location error of the signal source by an ESM is relatively small so that it might be able to track the platform of the signal source after detecting the signal source for three times.

Once the platform is tracked by a RWR or by an ESM, the combined PDS is able to identify the threat level of the signal source and then take actions. Since an ESM is sensitive to LPI time, the math model for LPI time estimation from equation (9) can be defined as

Table 1: Parameters of an airborne radar.

Radar parameters	Parameter values	Radar parameters	Parameter values
G_{ti}	34 dB	G_{rj}	34 dB
G_{RPj}	0 dB	λ	0.03 m
R_g	0.01	B_R	0.5 MHz
τ_0	2 μs	$P_t^{\max}$	20 kW
T_{ri}	1 ms	F_R	2 dB

Table 2: Parameters of a RWR and an ESM.

RWR parameters	Parameter values	ESM parameters	Parameter values
G_r	0 dB	$\bar{T}_f$	200 ms
G_{IP}	0 dB	τ_{sm}	1 ms
B_I	1 GHz	τ_{rem}	1 ms
F_I	5 dB	B_s	10 GHz
P_I	-60 dBmw	Δf_s	50 MHz

$$\begin{aligned}\max_{\text{SNR}_i, x} \quad & \bar{T}_{cn} \\ \text{s.t.} \quad & 0 < P_{\text{f}} \le P_{\text{fth}} \\ & 0 < P_{\text{d}} \le P_{\text{dth}} \\ & 0 < P_{ti} \le P_t^{\max} \\ & T_{ri} \le \tau_{ei} \le \frac{c\tau_0}{2v} \\ & \text{SNR}_{\text{net}}^{\text{th}} \le \text{SNR}_{\text{net}},\end{aligned} \tag{22}$$

where SNR_i and x refer to equations (3) and (9); $\bar{T}_{cn}$ denotes the average intercepted time for n times; P_{dth} and P_{fth} represent the predicted acceptable interception probability thresholds of a RWR and an ESM by NARS; P_{ti}, T_{ri}, and τ_{ei} are emission power, the minimum dwell time, and dwell time of the ith radar node; $P_t^{\max}$ is the maximum emission power of each radar node; c is light speed; τ_0 is pulse width and $\tau_0 \le \Delta\tau_e$; and $\text{SNR}_{\text{net}}^{\text{th}}$ is predicted the minimum detection SNR by NARS:

$$\begin{aligned}P_d &= \max P_{di}, \\ P_f &= \max P_{fi}, \\ &\text{for } i = 1, 2, \cdots, N_{\text{t}},\end{aligned} \tag{23}$$

where P_{di} and P_{fi} denote predicted interception probabilities of a RWR and an ESM of the ith radar node.

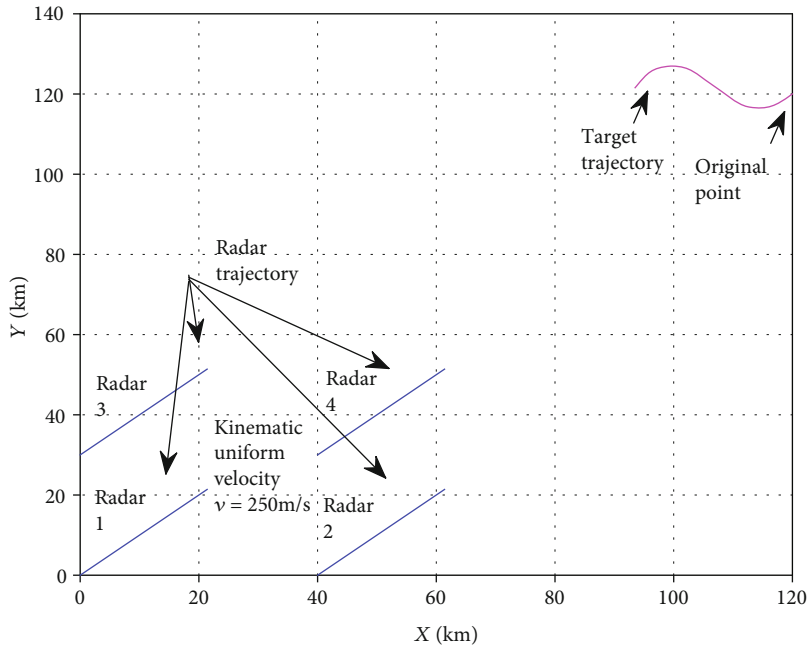

Figure 1: Trajectories of NARS and target on a planar scene.

Table 3: Maneuvering process of target.

Time	State equations
0~5	$F_1^T = [1, T, 0, 0\,; 0, 1, 0, 0\,; 0, 0, 1, T\,; 0, 0, 0, 1]$
6~20	$F_2^T = [1, \Gamma_1, 0, \Gamma_2\,; 0, \Gamma_3, 0, \Gamma_4\,; 0, -\Gamma_2, 1, \Gamma_1\,; 0, -\Gamma_1, 0, \Gamma_3]$
21~35	$F_1^T = [1, T, 0, 0\,; 0, 1, 0, 0\,; 0, 0, 1, T\,; 0, 0, 0, 1]$
36~54	$F_3^T = [1, -\Gamma_1, 0, \Gamma_2\,; 0, \Gamma_3, 0, -\Gamma_4\,; 0, -\Gamma_2, 1, -\Gamma_1\,; 0, \Gamma_1, 0, \Gamma_3]$
55~100	$F_1^T = [1, T, 0, 0\,; 0, 1, 0, 0\,; 0, 0, 1, T\,; 0, 0, 0, 1]$
101~120	$F_2^T = [1, \Gamma_1, 0, \Gamma_2\,; 0, \Gamma_3, 0, \Gamma_4\,; 0, -\Gamma_2, 1, \Gamma_1\,; 0, -\Gamma_1, 0, \Gamma_3]$

SNR_i of a RWR corresponding to P_{di} can be defined as

$$\mathrm{SNR}_i = \frac{P_{ti} G_{ti} G_r \lambda_i^2 G_{IP}}{(4\pi)^2 k T_o F_I B_I L_{Ii} R_i^2}, \tag{24}$$

where G_{ti}, L_{Ii}, and R_i are main beam gain, propagation loss, and distance from the ith radar node to the RWR and G_r, B_I, F_I, and G_{IP} are antenna gain, bandwidth, noise coefficient, and processor gain of the RWR.

Assume that the distance between any two radar nodes of NARS is far less than that from NARS to the target. The Schleher intercept factor of NARS α_{net} [32] is used to evaluate the LPI state of NARS, that is,

$$\alpha_{\mathrm{net}} = \frac{R_{i\ \max}}{R_{\mathrm{net\ max}}}. \tag{25}$$

The NARS will be in LPI state confronting a RWR in the power domain when α_{net} is far less than 1:

$$R_{i\ \max} = \left(\frac{\left[\max\left(P_{ti} G_{ti} \lambda_i^2 / L_{Ii}\right)\right] G_r G_{IP}}{(4\pi)^2 P_I} \right)^{1/2},$$
$$R_{\mathrm{netmax}} \triangleq \left(\frac{\sigma_{\mathrm{net}} G_{\mathrm{net}}^2 G_{\mathrm{rpnet}}}{(4\pi)^3 L_{\mathrm{net}} P_{R\mathrm{net}}} \sum_{i=1}^{N_t} \frac{P_{ti} \tau_{ei}}{T_{ri}} \lambda_i^2 \right)^{1/4}, \tag{26}$$

where $R_{i\ \max}$ is the maximum intercepted distance of NARS by a RWR; R_{netmax} is an approximate maximum detection distance by NARS; P_I is the RWR's sensitivity; σ_{net}, G_{net}, G_{rpnet}, L_{net}, and $P_{R\mathrm{net}}$ are approximate equivalent RCS, antenna gain, processor gain, system loss, and sensitivity of NARS, respectively.

4. Simulations

Assuming that NARS is tracking a target equipped with combined PDS whose properties is partially known from electronic intelligence and early warning system. Let SN $R_{\mathrm{net}}^{\mathrm{th}} = 3$ dB, $P_{\mathrm{d}} = 0.9$, $P_{\mathrm{fa}} = 1 \times 10^{-6}$, and $\mathrm{SNR}_i = 15$ dB. Main beam width and propagation loss of each radar node are 1° and 0.0126 dB/km. Other simulation parameters are listed in Tables 1 and 2.

The scene of target tracking by NARS is illustrated in Figure 1, where target moves from (120 km, 120 km) to (90 km, 120 km); initial positions of four radars in NARS are (0 km, 0 km), (40 km, 0 km), (0 km, 30 km), and (40 km, 30 km), respectively. Four radars formed a square formation at the speed of 250 m/s moving towards the target along a line.

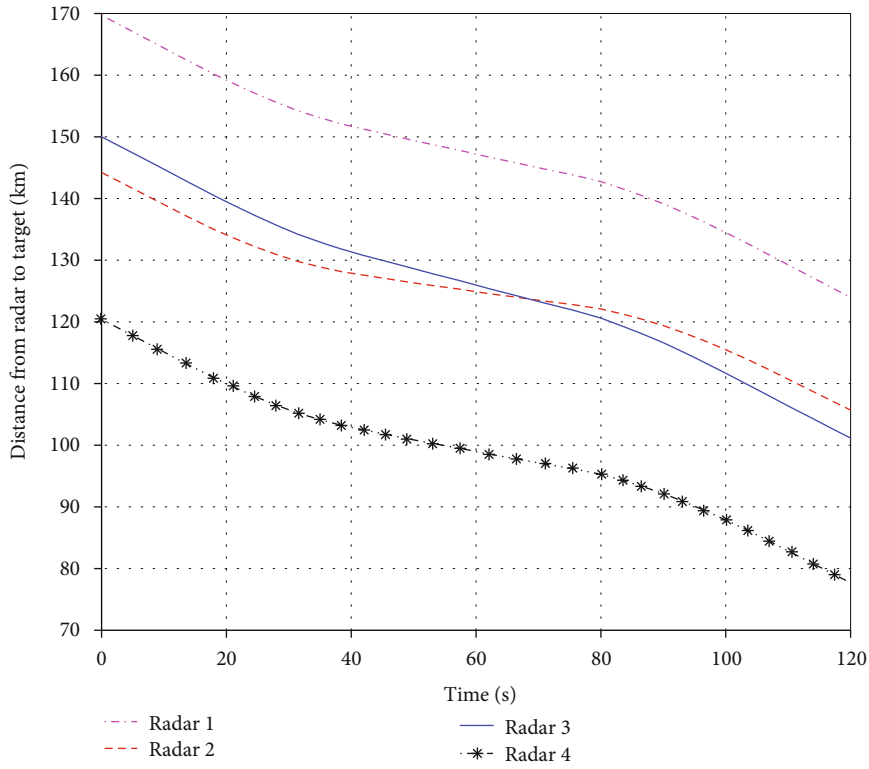

Figure 2: Time-based target tracking process by NARS.

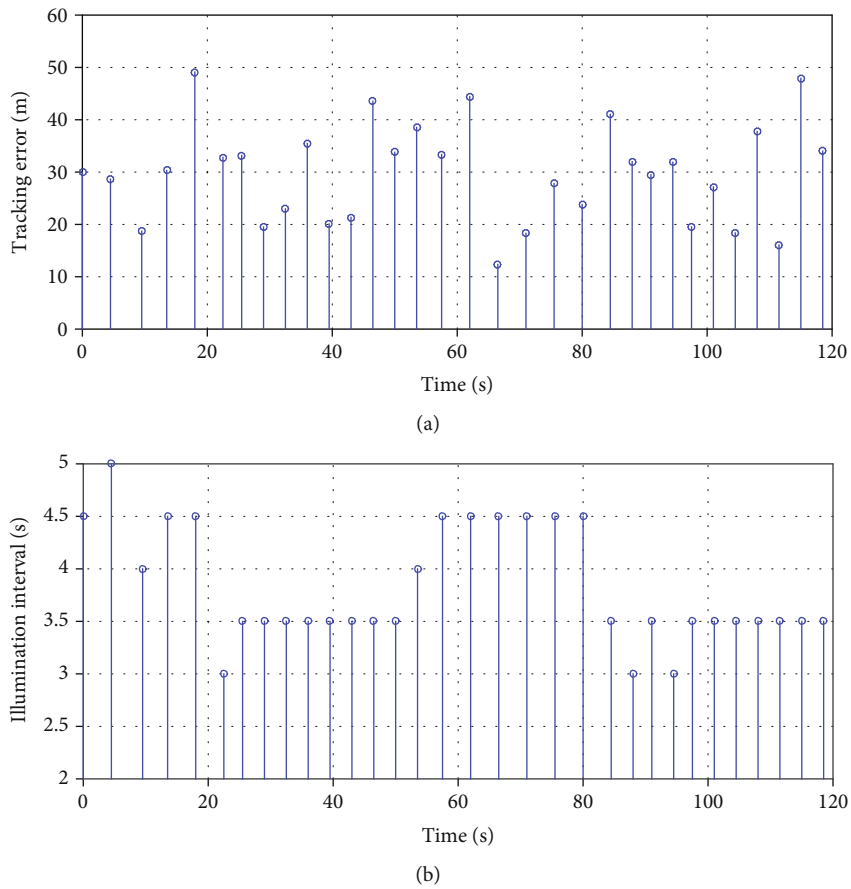

Figure 3: Time-based target tracking error and illumination interval by NARS.

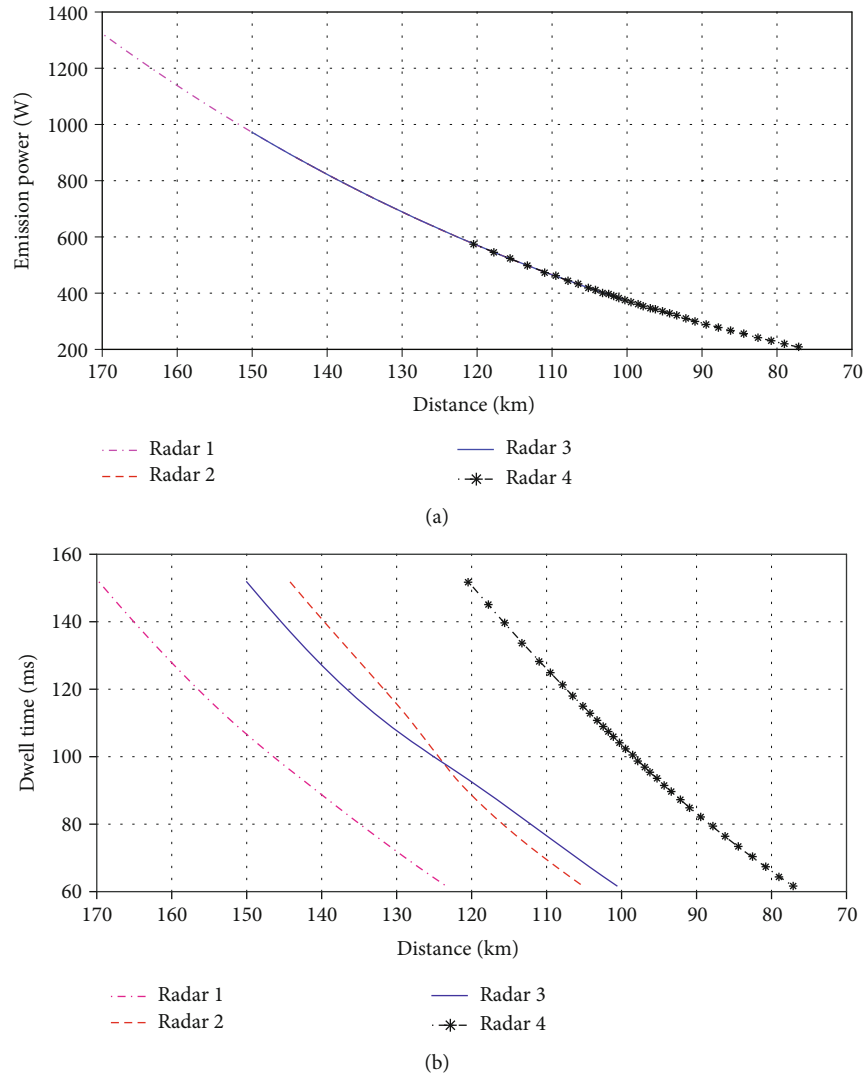

Figure 4: Distance-based emission power and dwell time of NARS.

From Table 3, there are three models and $\Delta T_{\min} = 1$ s, $\Delta T_{\max} = 5$ s. $\Gamma_1 = \sin(0.05\mathrm{T})/0.05$, $\Gamma_2 = [\cos(0.05T) - 1]/0.05$, $\Gamma_3 = \cos(0.05T)$, and $\Gamma_4 = \sin(0.05T)$. The covariance matrix of measure noise and system noise is $R_j^T(t) = [400,0\,;0,400]$ and $Q_j^T(t) = [10,0\,;0,10]$, respectively. Measure matrix $H_j^T = [1,0,0,0\,;0,0,1,0]$. Weighing matrix of system noise $G_j^T = [T^2/2,0\,;T,0\,;0,T^2/2\,;0,T]$. The initial error covariance matrix is $P_j(0) = \mathrm{diag}(460,100,460,100)$; the predefined upper limit of error covariance matrix is $\mathrm{tr}[P^{\mathrm{pred}}(t)] = 650$. The initial possibility matrix of each move model is $\mu_j(0) = [0.3,0.3,0.4]$. The model transform matrix is $\pi_{ij} = [0.9,0.05,0.05\,;0.1,0.8,0.1\,;0.05,0.15,0.8]$.

To improve LPI time of NARS, we take adaptively the sample interval and interactive multimodel Kalman filter to track the target. Figure 2 shows that the nearest distance between NARS and the target is 79 km. Figure 3 shows relationships between distance and sample intervals of four radars. Figure 3 shows that the maximum tracking error is less than 60 m; Figure 3(b) shows that the maximum sample interval is $5\Delta T$ min. Figures 4 and 5 show emission power and dwell time of each radar changed by target distance and target tracking time, respectively, during the target tracking process.

From Tables 1–3, with $T_{ri} = 1$ ms, $\tau_{\mathrm{rem}} = 1$ ms, $B_s = 10$ GHz, $\Delta f_s = 50$ MHz, and empirical values of possible short time $\bar{\tau}_{ei} = 150$ ms from Figures 4(b) and 5(b), and possible short time $\bar{T}_{rs} = (4.5 + 5 + 4)/3 = 4.5$ s from Figure 3(b). The preestimated P_f is about $\Delta f_s/B_s = 0.005$, and the mean of intercepted time of NARS by an ESM is about $\bar{T}_c = (200/150) \cdot 4.5 = 6$ s from equation (8).

Figure 6 shows the interception factor of NARS, while the receiver sensitivity of the airborne radar and the RWR is -140 dBmw and -60 dBmw, respectively, and SNR_i is 15 dB. From Figure 6, the LPI performance of NARS confronting a RWR is still smaller although the value of the interception factor is greater than that generated from Liao et al. [17]. The reason is that this paper has taken an ESM into account in Figure 7, which shows that the LPI time of NARS is much better than that of Liao et al. [17].

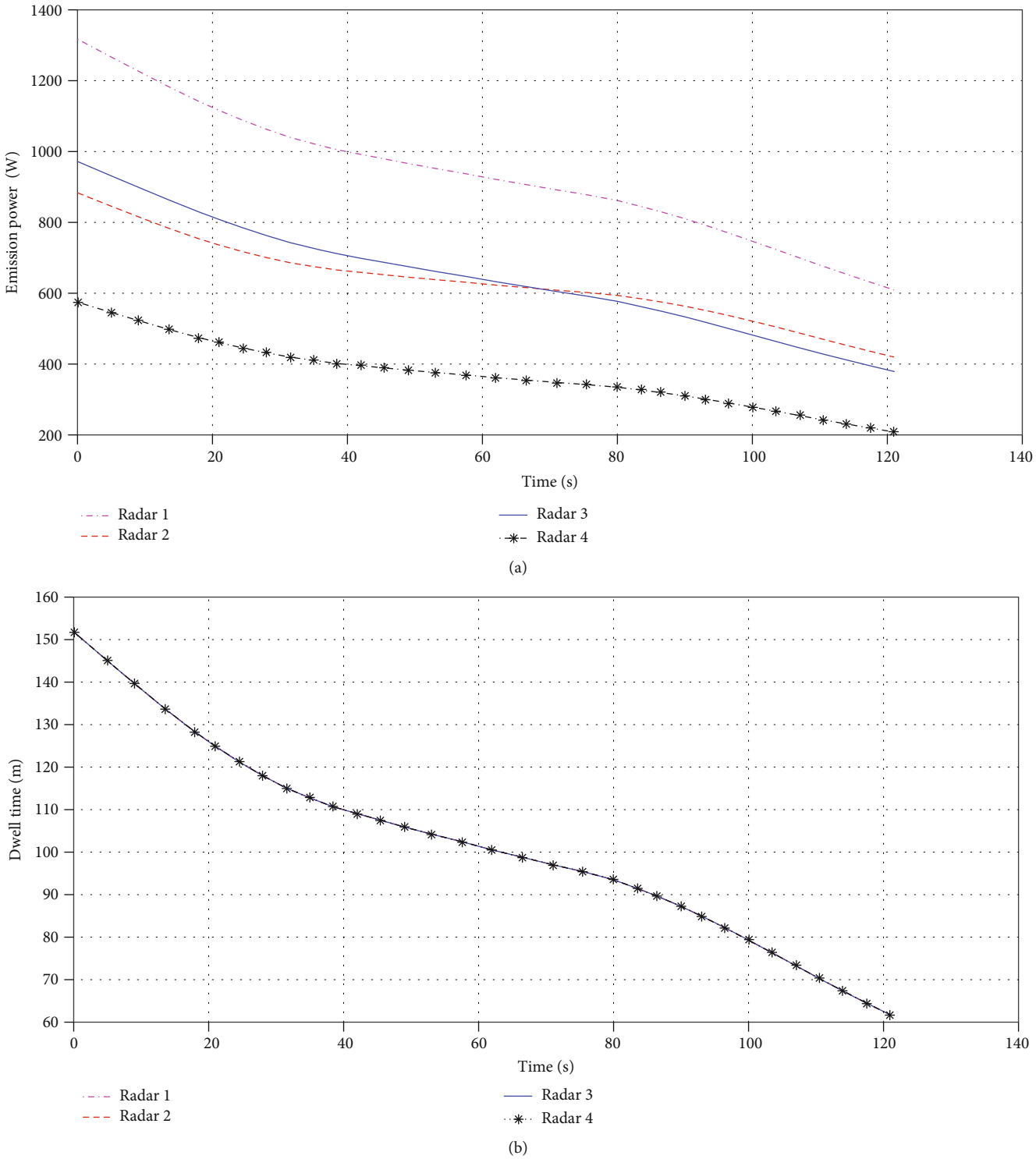

Figure 5: Time-based emission power and dwell time of NARS.

After 500 Monte Carlo experiments, Figures 7 and 8 shows cumulative intercepted time of all four radars in NARS by an ESM. Figure 7 shows that the average interception time for three times is 17 s; compared with the single radar, the interception time has increased by 6 times. Figure 8 is standard deviation which shows that the standard deviation of interception time for three times is 11 s. Because the three interception is independent of each other, the short average interception time for three times in equation (22) is about $\bar{T}_{cn} = 3 \cdot \bar{T}_c = 18$ s and the standard deviation is about $\sqrt{3}\bar{T}_c = 10.4$ s, which are close to 17 s and 11 s, respectively.

With the change of the detection SNR threshold of the RWR. Table 4 shows the changed interception factor from equation (25) and changed average time of being intercepted

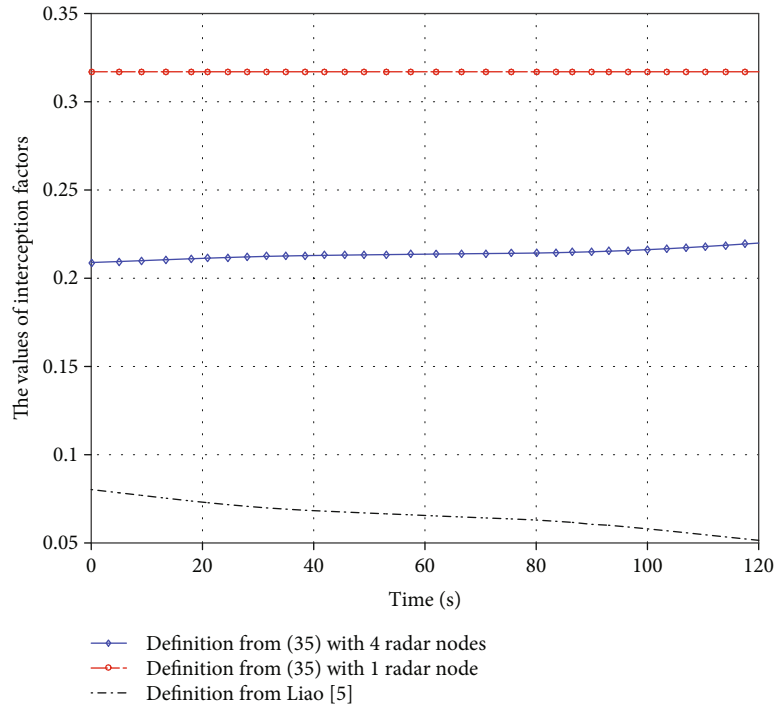

Figure 6: Time-based interception factor comparison confronting a RWR.

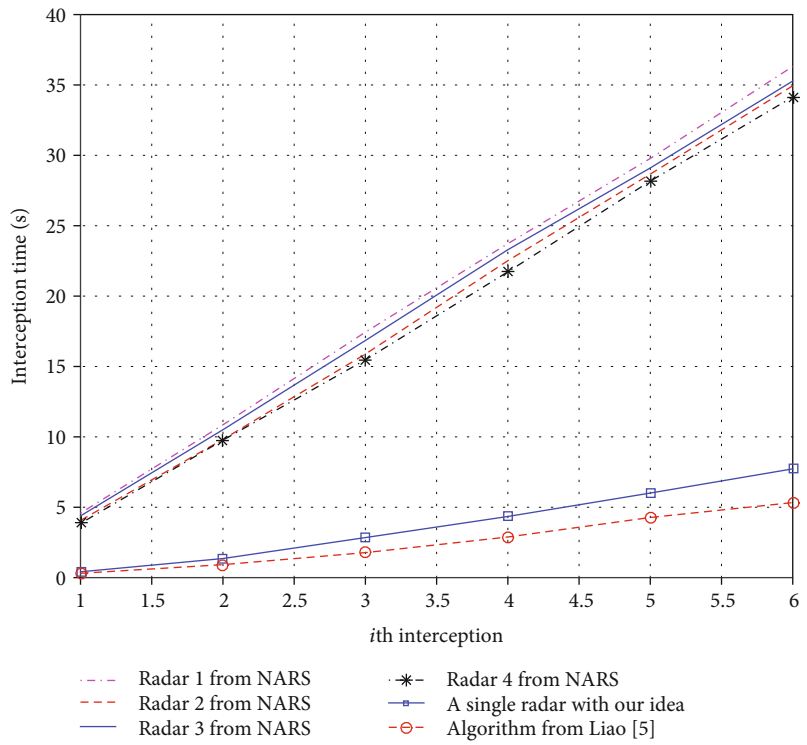

Figure 7: The mean of intercepted time of NARS by an ESM.

by three times. According to the data in Table 4, the ratio of the average time of being intercepted by three times to the interception factor is approximately linear to the detection SNR threshold of a RWR. However, if NARS could be located by a RWR once SNR is over a key threshold, the linear relationship in Table 4 would be not valid any more.

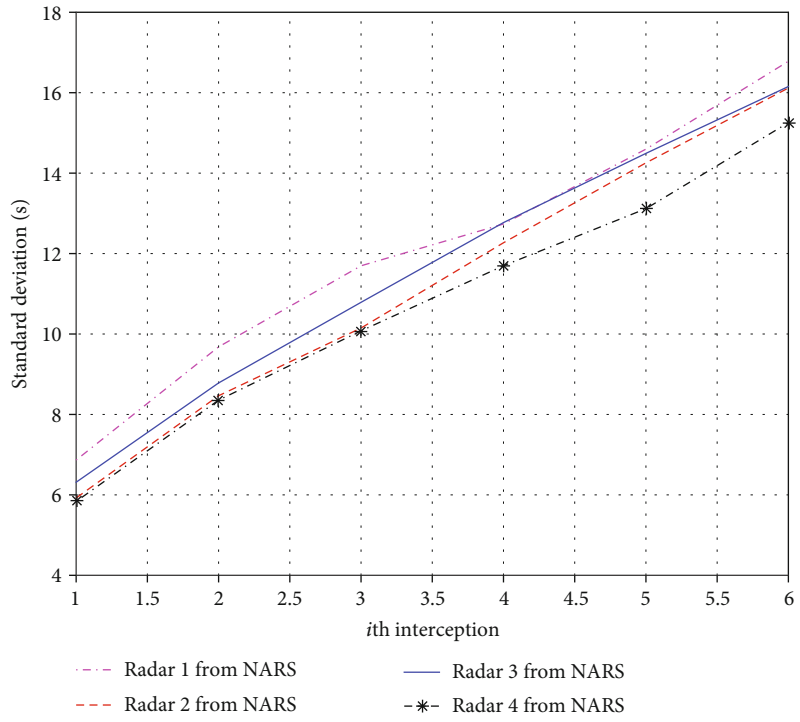

Figure 8: The standard deviation of intercepted time of NARS by an ESM.

Table 4: LPI time by a combined PDS with different SNR_i.

SNR_i threshold	Interception factor	Three-time interception
10 dB	0.1234	3.6676
12 dB	0.1553	7.4291
14 dB	0.1955	11.719
16 dB	0.2462	22.24
18 dB	0.3099	34.1784
20 dB	0.3902	50.9894
22 dB	0.4912	72.7639
24 dB	0.6184	124.5220

5. Conclusion

In order to study LPI time of NARS under the circumstances of a PDS, we modelled a PDS as the combination of a RWR and an ESM. The model makes the tracking task between aircrafts and target more realistic. Generally, NARS is required to decrease emission power to elude a RWR while increasing emission power to elude an ESM. For that inherent contradiction, LPI time is important to guide NARS to control its radiation power and time simultaneously and to avoid the threat from a combined PDS. This paper proposes a simplified math model to estimate LPI time of NARS when the parameters of combined PDS are partially known. Simulation results illustrate that the simultaneous management of radiation power and time can help NARS against combined PDS interception.

Data Availability

The data used to support the conclusion of this study are available in Section 4.

Conflicts of Interest

The authors declare that they have no competing interests.

Authors' Contributions

All authors equally contributed to this paper.

Acknowledgments

This research is supported by the Aeronautical Science Foundation of China (Grant Nos. 2017ZC52036 and 20172752019), National Natural Science Foundation of China under Grant 61801212, and Natural Science Foundation of Jiangsu Province under Grant BK20180423.

References

[1] M. Kobayashi, "Stealth technology based on active EA(electronic attack)," Technical Report of Ieice Sane, 2013.

[2] J. Chen, F. Wang, J. Zhou, and C. Shi, "Spectral distribution of Wigner matrices in finite dimensions and its application to LPI performance evaluation of radar waveforms," *IEICE Transactions on Fundamentals of Electronics, Communications and Computer Sciences*, vol. E100.A, no. 9, pp. 2021–2025, 2017.

[3] Y. M. Hwang, J. H. Jung, K. Y. Kim et al., "Energy-efficient resource allocation strategy for low probability of intercept

and anti-jamming systems," *IEICE Transactions on Fundamentals of Electronics, Communications and Computer Sciences*, vol. E100.A, no. 11, pp. 2498–2502, 2017.

[4] Z. Zhang and J. Zhu, "A novel power control method of phased array radar based on the predicted tracking Cramér-Rao Lower Bounds," in *2015 IEEE International Conference on Information and Automation*, pp. 2888–2891, Lijiang, China, 2015.

[5] J. Kamble, I. A. Pasha, and M. Madhavilatha, "Design of HRR detection system for measurement of RF signal power," in *2016 10th International Conference on Intelligent Systems and Control (ISCO)*, pp. 1–5, Coimbatore, India, 2016.

[6] C. Shi, F. Wang, M. Sellathurai, and J. Zhou, "Low probability of intercept based multicarrier radar jamming power allocation for joint radar and wireless communications systems," *IET Radar, Sonar & Navigation*, vol. 11, no. 5, pp. 802–811, 2017.

[7] X. Wang, W. Yi, M. Xie, and L. Kong, "A joint beam and dwell time allocation strategy for multiple target tracking based on phase array radar system," in *2017 20th International Conference on Information Fusion (Fusion)*, pp. 1–5, Xi'an, China, 2017.

[8] C. Shi, J. Zhou, and F. Wang, "Adaptive resource management algorithm for target tracking in radar network based on low probability of intercept," *Multidimensional Systems and Signal Processing*, vol. 29, no. 4, pp. 1203–1226, 2018.

[9] H. Godrich, A. P. Petropulu, and H. V. Poor, "Power allocation strategies for target localization in distributed multiple-radar architectures," *IEEE Transactions on Signal Processing*, vol. 59, no. 7, pp. 3226–3240, 2011.

[10] P. Chavali and A. Nehorai, "Distributed data association for multiple-target tracking using game theory," in *2013 IEEE Radar Conference*, pp. 1–6, Canada, September 2013.

[11] H. Gao, J. Wang, and X. Zhang, "Resource allocation in MIMO radar with widely separated antennas for multi-target detection," in *2014 IEEE Radar Conference*, pp. 1–6, Lille, France, October 2014.

[12] M. Barbary and P. Zong, "Optimisation for stealth target detection based on stratospheric balloon-borne netted radar system," *IET Radar, Sonar & Navigation*, vol. 9, no. 7, pp. 802–816, 2015.

[13] C. Shi, J. Zhou, and F. Wang, "LPI based resource management for target tracking in distributed radar network," in *2016 IEEE Radar Conference (RadarConf)*, pp. 1–5, Philadelphia, PA, USA, May 2016.

[14] D. Liu, F. Wang, C. Shi, and J. Zhang, "LPI based optimal power and dwell time allocation for radar network system," in *2016 CIE International Conference on Radar (RADAR)*, pp. 921–925, Guangzhou, China, October 2016.

[15] F. Wang, S. Yu, C. Shi, and M. Sellathurai, "LPI time-based TMS against high-sensitivity ESM," *IET Radar, Sonar & Navigation*, vol. 12, no. 12, pp. 1509–1516, 2018.

[16] X. Song, P. Willett, and S. Zhou, "Optimal power allocation for MIMO radars with heterogeneous propagation losses," in *2012 IEEE International Conference on Acoustics, Speech and Signal Processing (ICASSP)*, pp. 2465–2468, Kyoto, Japan, 2012.

[17] W. W. Liao, T. Cheng, and Z. S. He, "A target tracking algorithm for RF stealth performance optimization of MIMO radar," *Chinese Journal of Aeronautics*, vol. 35, no. 4, pp. 1134–1141, 2014.

[18] S. W. Yang, T. Cheng, and Z. S. He, "Algorithm of radio frequency stealth for MIMO radar in searching mode," *Journal of Electronics and Information Technology*, vol. 36, no. 5, pp. 1017–1022, 2014.

[19] Y. Yu, S. Sun, R. N. Madan, and A. Petropulu, "Power allocation and waveform design for the compressive sensing based MIMO radar," *IEEE Transactions on Aerospace and Electronic Systems*, vol. 50, no. 2, pp. 898–909, 2014.

[20] N. Garcia, A. M. Haimovich, M. Coulon, and M. Lops, "Resource allocation in MIMO radar with multiple targets for non-coherent localization," *IEEE Transactions on Signal Processing*, vol. 62, no. 10, pp. 2656–2666, 2014.

[21] B. Ma, H. Chen, B. Sun, and H. Xiao, "A joint scheme of antenna selection and power allocation for localization in MIMO radar sensor networks," *IEEE Communications Letters*, vol. 18, no. 12, pp. 2225–2228, 2014.

[22] J. Yan, H. Liu, B. Jiu, B. Chen, Z. Liu, and Z. Bao, "Simultaneous multibeam resource allocation scheme for multiple target tracking," *IEEE Transactions on Signal Processing*, vol. 63, no. 12, pp. 3110–3122, 2015.

[23] J. Yan, B. Jiu, H. Liu, B. Chen, and Z. Bao, "Prior knowledge-based simultaneous multibeam power allocation algorithm for cognitive multiple targets tracking in clutter," *IEEE Transactions on Signal Processing*, vol. 63, no. 2, pp. 512–527, 2015.

[24] Z. Xiang and B. Chen, "Optimal frequency increment selection in frequency diverse multiple-input–multiple-output radar," *IET Radar, Sonar & Navigation*, vol. 10, no. 8, pp. 1431–1438, 2016.

[25] B. Tang, J. Tang, and Y. Zhang, "Design of multiple-input–multiple-output radar waveforms for Rician target detection," *IET Radar, Sonar & Navigation*, vol. 10, no. 9, pp. 1583–1593, 2016.

[26] N. Goodman and D. Bruyere, "Optimum and decentralized detection for multistatic airborne radar," *IEEE Transactions on Aerospace and Electronic Systems*, vol. 43, no. 2, pp. 806–813, 2007.

[27] D. Rong, L. Na, W. Xiang, and W. An, "CSMA-BT protocol for intra-flight data link," in *2012 International Conference on Industrial Control and Electronics Engineering*, pp. 1907–1910, Xi'an, China, 2012.

[28] M. I. Skolnik, *Introduction to Radar Systems*, McGraw Hill Book Co., 2001.

[29] B. R. Mahafza, *Radar Systems Analysis and Design Using MATLAB*, Publishing House of Electronics Industry, Beijing, China, 2nd edition, 2008.

[30] A. De Martino, *Introduction to Modern EW Systems*, Artech House, 2012.

[31] H. A. P. Blom and Y. Bar-Shalom, "The interacting multiple model algorithm for systems with Markovian switching coefficients," *IEEE Transactions on Automatic Control*, vol. 33, no. 8, pp. 780–783, 1988.

[32] C. Shi, J. Zhou, and F. Wang, "Low probability of intercept optimization for radar network based on mutual information," in *2014 IEEE China Summit & International Conference on Signal and Information Processing (ChinaSIP)*, pp. 683–687, Xi'an, China, 2014.